Early interaction between Fe–Cr alloy metallic interconnect and Sr-doped $LaMnO_3$ cathodes of solid oxide fuel cells

S.P. Jiang,[a] Sam Zhang,[b] and Y.D. Zhen
Fuel Cells Strategic Research Program, School of Mechanical and Production Engineering, Nanyang Technological University, Singapore 639798

(Received 25 October 2004; accepted 15 December 2004)

The initial stages of the interaction between the Fe–Cr alloy metallic interconnect and Sr-doped $LaMnO_3$ (LSM) electrode of solid oxide fuel cells (SOFC) were investigated under cathodic polarization at the temperature range of 700–900 °C. Cr deposits on the Y_2O_3–ZrO_2 (YSZ) electrolyte surface increased with the polarization time. However, it was observed that at the early stages of the reaction, there is no preferential Cr deposition at the three-phase boundary areas at the LSM electrode/YSZ electrolyte interface region. With the decrease of the temperature the Cr deposition reduced significantly, probably due to the significant reduction in the partial pressure of the gaseous Cr species and the cationic diffusivities in the LSM electrode. The results clearly demonstrated that the deposition of Cr species at the LSM electrode/YSZ electrolyte is basically a chemical reaction and kinetically controlled by the nucleation reaction between the gaseous Cr species and the Mn^{2+} species generated under cathodic polarization.

I. INTRODUCTION

The function of the interconnect in solid oxide fuel cells (SOFCs) is to connect individual cells electrically in series to form stacks to generate the desired power output with high voltage. Thus, the interconnect materials should have high electrical conductivity and negligible ionic conductivity and should be chemically and structurally stable under both air and fuel environment. There are basically two types of interconnect materials commonly used in SOFCs: doped $LaCrO_3$-based ceramic materials and high-temperature oxidation resistance metallic materials.[1] Significant progress has been made in the decreasing of the operating temperature of a SOFC to 600–800 °C due to the significant reduction of the electrolyte thickness[2] and the development of new electrode materials.[3–5] The reduced operation temperature of SOFC greatly increases the feasibility of using low-cost metallic interconnect materials.[6–9] Compared to the ceramic interconnect materials, metals have high electronic and thermal conductivity, negligible ionic conductivity, good machinability and low cost.

Alloys of high-temperature oxidation resistance used as interconnect in SOFC generally contain chromium as an alloying element to form a protective chromium oxide scale (Cr_2O_3). At high temperatures volatile Cr species such as high valent vapor Cr species [e.g., CrO_3 and $Cr(OH)_2O_2$] will be generated over the oxide scale layer in oxidizing atmospheres.[10,11] It is well known that without effective protective coatings, the gaseous Cr species generated can cause rapid performance deterioration of (La,Sr)MnO_3 (LSM)-based electrodes for the O_2 reduction reaction.[12–16] However, there are considerable disagreements on the degradation mechanism of the chromium species on the O_2 reduction reaction. Taniguchi et al.[12] and Badwal et al.[13] considered that the degradation of Cr species is closely related to the oxygen activity at the electrode/electrolyte interface. In another words, the deposition of Cr is mainly caused by the electrochemical reduction of gaseous Cr species to solid Cr_2O_3 phase in competition with the O_2 reduction reaction.[17] This appears to be supported by the thermodynamic compatibility of the electrochemical reduction of high valent Cr species and O_2 reduction reaction under the SOFC operation conditions.[10] However, our systematic studies of the Cr deposition processes on various SOFC cathodes such as LSM, (LaSr)$(CoFe)O_3$, and Pt clearly demonstrate that kinetically the deposition process of Cr species at LSM electrode is dominated by the chemical dissociation of the high valent Cr species.[18–20] The deposition reaction is most likely initiated by the

[a]Address all correspondence to this author.
e-mail: mspjiang@ntu.edu.sg
[b]This author was an editor of this journal during the review and decision stage. For the *JMR* policy on review and publication of manuscripts authored by editors, please refer to http://www.mrs.org/publication/jmr/policy.html.
DOI: 10.1557/JMR.2005.0101

nucleation of manganese species (e.g., Mn^{2+}) generated under cathodic polarization or at high temperatures.

In this paper, the Cr deposition processes at LSM electrodes were studied at different temperatures and special attention was paid to the early stage of the reaction. The results again support the view that the Cr species is basically deposited through the chemical dissociation under SOFC operation conditions.

II. EXPERIMENTAL

Zirconia electrolyte disks were prepared from 8 mol% Y_2O_3-doped ZrO_2 powder (YSZ; Tosoh, Shiba, Japan) by die pressing, followed by sintering at 1500 °C for 4 h in air. The thickness and diameter of the sintered electrolyte disks were about 1 mm and 19 mm, respectively. The A-site nonstoichiometry $La_{0.72}Sr_{0.18}MnO_3$ (LSM) electrode powders were prepared by co-precipitation and calcined at 1000 °C in air. The A-site deficient LSM composition was chosen to avoid the resistive phase formation at the LSM/YSZ interface.[21] The LSM cathode coating was applied to the yttria-stabilized zirconia (YSZ) electrolyte by screen printing, followed by sintering at 1150 °C for 2 h in air. The electrode thickness was ~20 μm, and the electrode area was 0.5 mm^2. Pt paste (Ferro Corporation, Cleveland, OH) was painted on the opposite side of the working electrode to serve as the counter and reference electrodes. The counter electrode was symmetrical to the LSM electrode and the reference electrode was painted as a ring around the counter electrode. The distance between the counter electrode and the ring reference electrode was approximately 4 mm.

The chromia-forming alloy interconnect was a commercial Fe–Cr alloy RA446 (23-27%Cr, 1.5%Mn, 1%Si, 0.2%C, 0.12%N and the remaining Fe; Rolled Alloy Co., Ontario, Canada). RA446 is high chromium ferric heat resistance alloy with excellent resistance to oxidation. The melting temperature of the alloy is in the range of 1448–1478 °C. After oxidation at 900 °C in air, an oxide scale was formed and the morphology of the oxide scale was characterized by the dense packed and well-defined $(Cr,Mn)_3O_4$ spinels and Cr_2O_3 oxides. The alloys were machined into coupons (12 × 12 × 4 mm) with channels (1.2 × 1.2 mm) cut on one side of the coupon. Air was directed to the channels through an alumina tube. Two Pt wires were spot-welded to the coupon to serve as the voltage and current probes, respectively. There was no Pt mesh placed between the chromia-forming alloy and the electrode coating. In this arrangement, the chromia-forming alloy also acted as a current collector. Air (industrial grade, H_2O content <3 ppm) was used without further drying. The air flow rate was controlled at 100 ml min^{-1}. Figure 1 shows the cell configuration and the arrangement of the Fe–Cr alloy interconnect.

The polarization behavior of the LSM electrode was

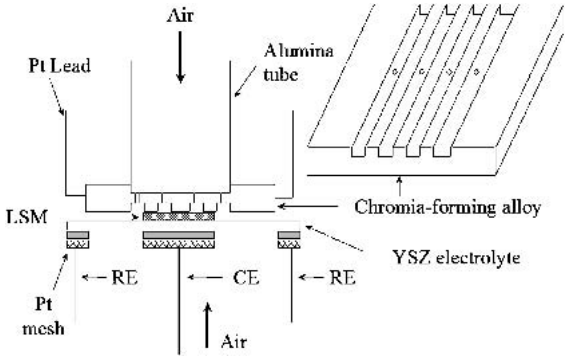

FIG. 1. Cell configuration and the arrangement of the Fe–Cr alloy interconnect.

carried out under a constant current density of 200 mA cm^{-2} in air at 700, 800, and 900 °C, respectively. The polarization potential ($E_{cathode}$) was measured against the Pt air reference electrode. The current passage was interrupted from time to time to make electrochemical impedance spectroscopy (EIS) measurements. A Solartron 1260 frequency response analyzer in conjunction with a 1287 electrochemical interface was used for the EIS measurement. EIS curves were measured in the frequency range of 0.1 Hz to 100 kHz with the amplitude of 10 mV at open circuit. Electrode ohmic resistance (R_Ω) was measured from the high frequency intercept and the electrode interface (polarization) resistance (R_E) was directly obtained from the difference between the high-frequency and the low-frequency intercept on the impedance spectra. Thus overpotential (η) can be obtained from $E_{cathode}$ and R_Ω by the following equation

$$E_{cathode} = \eta + jR_\Omega \quad , \tag{1}$$

where j is the current density.

Scanning electron microscopy (SEM; Leica 360, Wetzlar, Germany) and x-ray energy dispersion spectroscopy (EDS; Oxford, UK) were used to examine the LSM/YSZ interface morphology and the elemental distribution of the deposits. The LSM electrode was removed carefully by a doctor blade to examine the YSZ electrolyte surface in contact with the LSM electrode coating. In some cases, the LSM coating was removed by 20% HCl acid treatment, followed by washing with de-ionized water. It was found that acid treatment by 20% HCl solution mainly removed the LSM coating and majority of the Cr deposits were still intact on the YSZ electrolyte surface after the 20% HCl acid treatment.

III. RESULTS

Figure 2 shows the SEM micrographs of the YSZ electrolyte surface in contact with the LSM electrode coating in the presence of chromia-forming alloy at 900 °C after cathodic polarization for different periods. The LSM

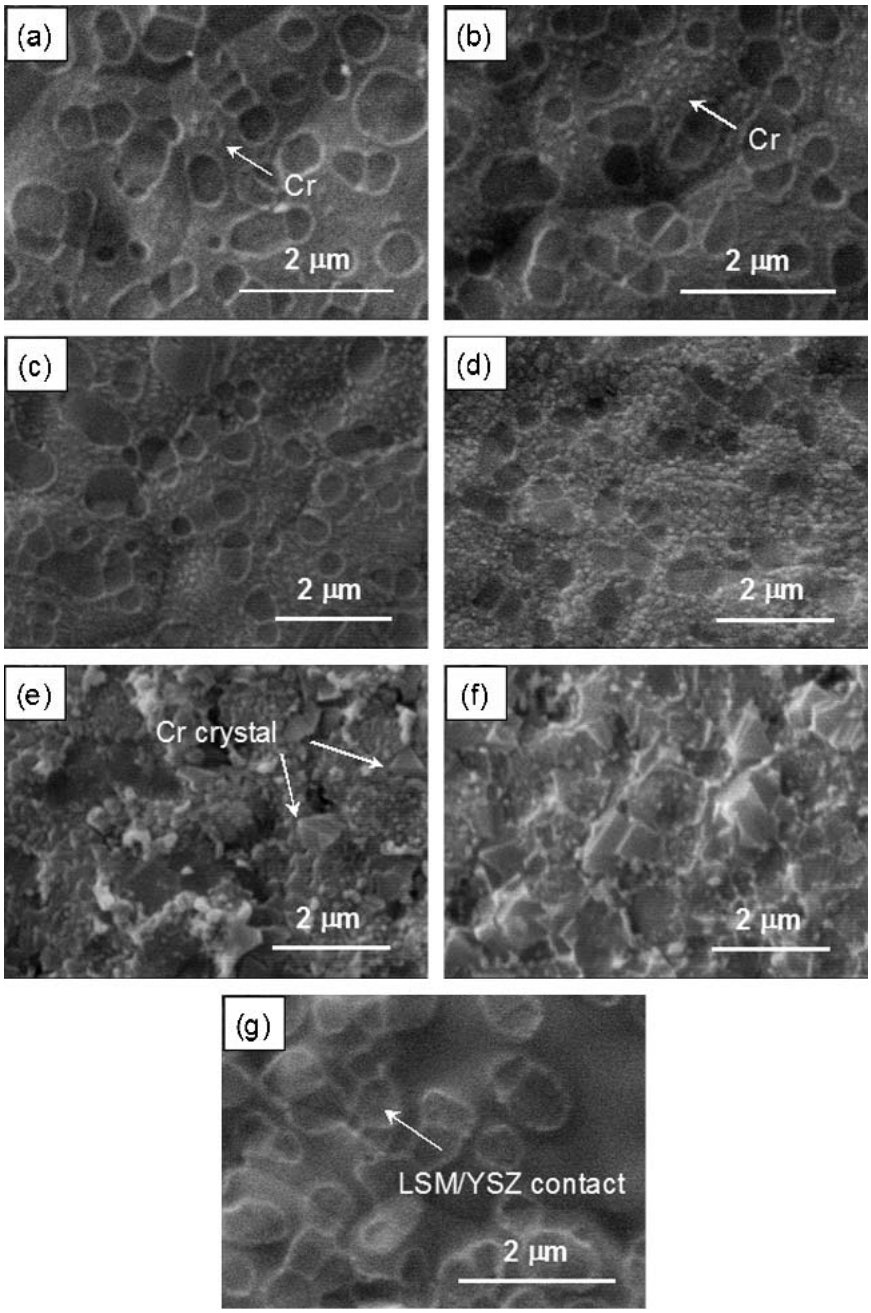

FIG. 2. SEM micrographs of the YSZ electrolyte surface in contact with the LSM electrode coating in the presence of a Fe–Cr alloy at 900 °C after cathodic polarization for (a) 5 min, (b) 15 min, (c) 30 min, (d) 4 h, (e) 20 h, and (f) 50 h. The YSZ surface in contact with LSM electrode after polarization at 200 $mAcm^{-2}$ at 900 °C for 4 h in the absence of Fe–Cr alloy is shown in (g). The LSM electrode coating was removed by HCl acid treatment.

electrode coating was removed by the HCl acid treatment. In comparison, YSZ surface in contact with a LSM electrode after the cathodic current passage at 200 $mAcm^{-2}$ and 900 °C for 4 h in the absence of Fe–Cr alloy is shown in Fig. 2. The convex rings were contact areas between LSM particles and the YSZ electrolyte surface [Fig. 2(g)], formed during the electrode sintering steps.[22] After cathodic current passage for 5 min, there was formation of the isolated fine Cr grains at areas between the LSM particles [Fig. 2(a)]. As the cathodic current passage time increased to 15 min, the density of the fine grains increased [Fig. 2(b)]. However, the fine grains had no preferential deposition at the three phase boundaries (i.e., the convex ring region). Rather, the deposition of the fine Cr grains was random, simply filling the space between the LSM grains with the increase in the cathodic polarization time [Figs. 2(c) and 2(d)]. As the cathodic current passage increased to 20 and 50 h,

the fine grains grew into crystals with distinct facets [Fig. 2(e) and 2(f)]. The crystals were most likely due to the formation of $(CrMn)_3O_4$ phases, as shown in earlier work.[18]

Figure 3 shows the SEM micrographs of the LSM electrode and the YSZ electrolyte surface after the LSM coating was removed by the HCl acid treatment. The LSM electrode was cathodically polarized for 20 h at 900 °C. The formation of deposit band 40–50 μm wide was clearly visible at the edge of the LSM electrode, similar to the deposition ring observed for the O_2 reduction on the LSM electrode/3mol% Y_2O_3–ZrO_2 electrolyte system.[18] A wavelike band was also observed on the YSZ electrolyte surface under the rib of the interconnect [Fig. 3(a)]. On the YSZ electrolyte surface, there was a formation of dense deposit layer at the areas close to the LSM electrode coating [Fig. 3(b)]. There was also formation of distinctive crystals on the LSM surface at the edge of the electrodes. After the removal of the LSM electrode coating, cotton-like particles with no distinct facets were seen on the YSZ electrolyte surface at areas close to the edge of the LSM electrode [Figs. 3(c) and 3(d)]. The Cr deposition on the YSZ electrolyte surface also depends on the contact surface of the interconnect. Clearly the Cr deposition on the YSZ electrolyte surface under the rib of the interconnect [Fig. 3(e)] is more significant than that under the channel of the interconnect [Fig. 3(f)]. The areas under the rib or channel were easily identified from the contact mark of the Fe–Cr alloy left on the LSM electrode coating. This again indicates the significant effect of the interconnect flow field on the deposition of Cr species on the LSM/YSZ system.[19]

Figure 4 is the EDS analysis of the Cr deposits of Fig. 3. The composition of the cotton-like particles formed on the YSZ surface close to the edge of the LSM

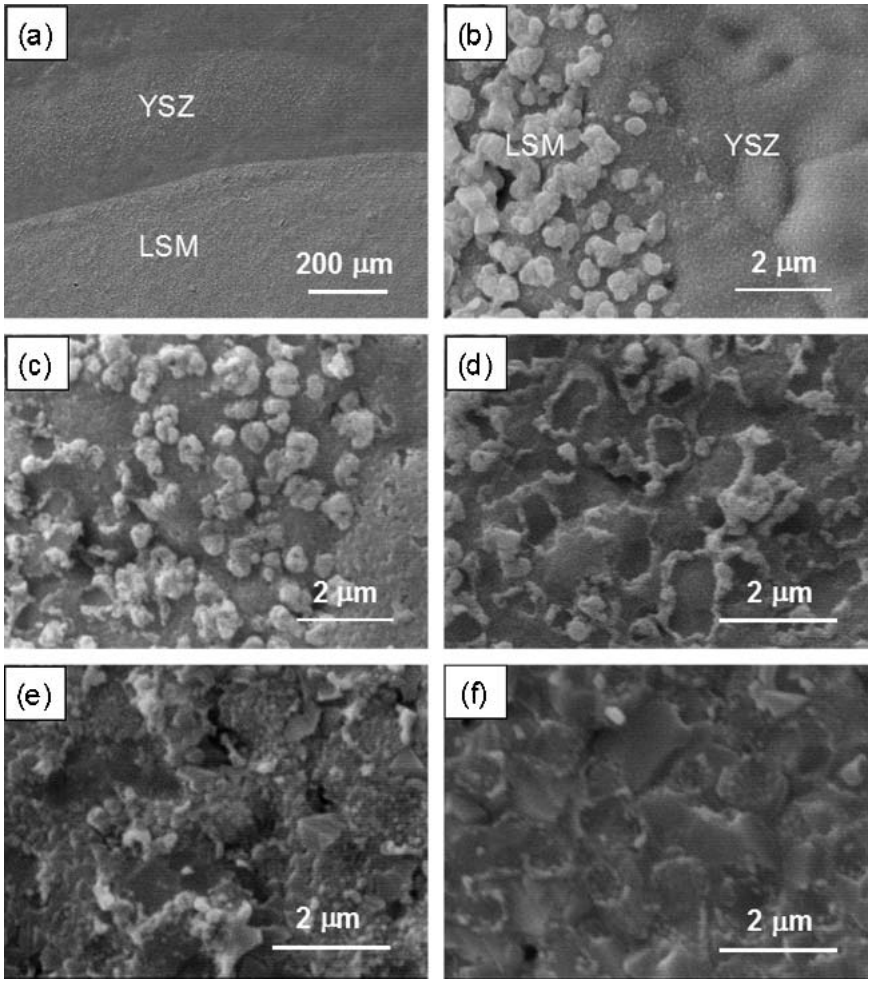

FIG. 3. SEM micrographs of LSM electrode and YSZ electrolyte surface after the cathodic current passage for 20 h at 900 °C in the presence of Fe–Cr alloy. The LSM coating was removed by HCl acid treatment. (a) An overview of the coating, showing the formation of deposit band. (b) The edge of the LSM electrode before the removal of the coating. (c) The edge of the LSM electrode after the removal of the coating. (d) YSZ surface in contact with LSM, ~20 μm from the edge of LSM electrode. (e) Center of the YSZ surface in contact with LSM under the rib of the interconnect. (f) Center of the YSZ surface in contact with LSM under the channel of the interconnect.

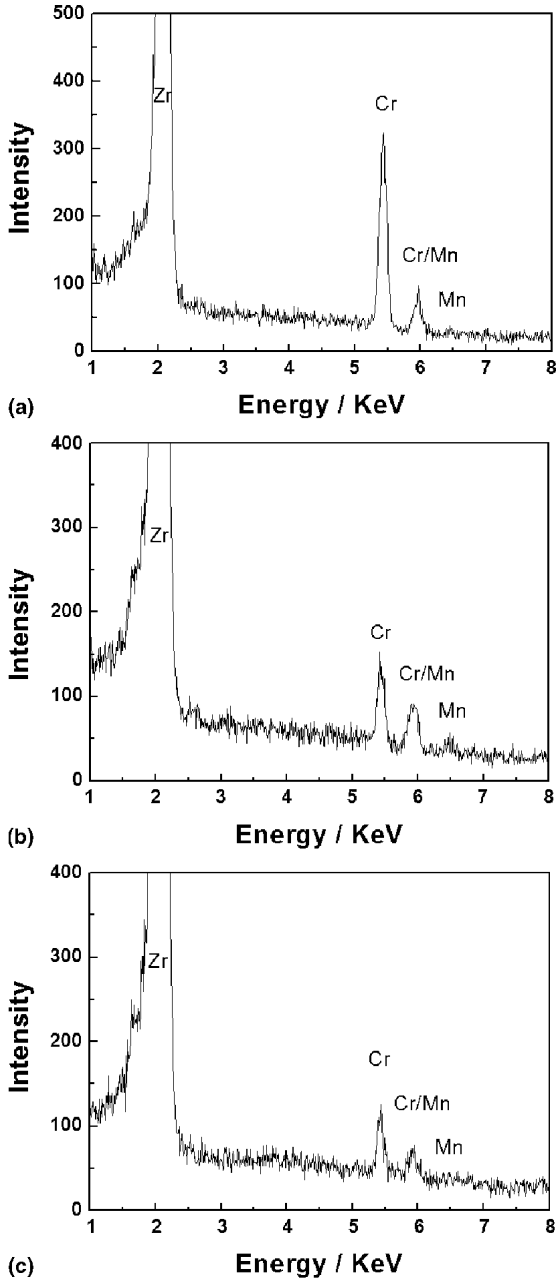

FIG. 4. EDS patterns of (a) cotton-like deposits of Figs. 3(c) and 3(d), (b) grains and crystal-like deposits under the rib of the interconnect, and (c) grains and crystal-like deposits under the channel of the interconnect.

electrode coating [Figs. 3(c) and 3(d)] mainly consists of Cr with very small amount of Mn [Fig. 4(a)]. This shows that the cotton-like particles are most likely Cr_2O_3. On the YSZ surface areas away from the edge of the LSM electrodes, the EDS pattern clearly shows the existence of Cr and Mn for the deposits under the rib [Fig. 4(b)] and the channel [Fig. 4(c)] of the interconnect. This indicates that crystals formed on the YSZ surface under the rib and the channel of the interconnect are most likely $(CrMn)_3O_4$ spinels.

It was found that the Cr deposition on the YSZ electrolyte surface not in direct contact with LSM electrode coating was also significantly related to the flow field of the interconnect. Figure 5 shows the SEM micrographs of the Cr deposits on the YSZ electrolyte surface not in direct contact with the LSM coating under the rib of the interconnect after cathodic current passage at 900 °C for 20 h. Figure 6 shows the corresponding Cr deposition on the YSZ electrolyte surface under the channel of the interconnect. Clearly, the deposition of Cr is far more substantial on the YSZ electrolyte surface under the rib of the interconnect than that under the channel of the interconnect. For the YSZ electrolyte surface under the rib of the interconnect, Cr was deposited as far as 250 μm away from the edge of the LSM electrode [Fig. 5(d)] while in the case of the YSZ surface under the channel of the interconnect, the corresponding YSZ electrolyte surface with visible Cr deposits was approximately 70 μm away from the edge of the LSM electrode [Fig. 6(e)]. Cr deposits were observed on the concave surface of the YSZ grains but not on the convex surface of the YSZ grains. The deposits on the YSZ electrolyte surface in both cases mainly contain Cr as shown by the EDS analysis of the deposits under the rib and the channel of the interconnect (Fig. 7). This shows that the Cr deposits on the YSZ electrolyte surface were most likely Cr_2O_3 oxides. Similar deposition of Cr patterns on the YSZ electrolyte surface under the rib and the channel of the interconnect was also observed for the reaction with no air flow.[19]

The deposition of Cr species was also studied at different temperatures. Figure 8 shows the SEM micrographs of the YSZ electrolyte surface in contact with the LSM electrode after cathodic current passage at 200 $mAcm^{-2}$ for 20 h at different temperatures. The SEM pictures shown in the figure were taken on the YSZ surface under the rib of the Fe–Cr interconnect and LSM electrode coating was carefully removed by a sharp doctor blade after the testing. Figure 9 shows the corresponding EDS patterns of the deposits formed at different temperatures. At 900 °C, the YSZ electrolyte surface in contact with the LSM coating was almost completely covered by fine grains (~0.05 μm) and large crystals (~0.8 μm) [Fig. 8(a)]. The crystals formed have distinct facets and were seemed to grow from the fine grains. EDS analysis of crystals revealed the existence of Cr and Mn [Fig. 9(a)], indicating that the crystals were $(Cr,Mn)_3O_4$ spinels.[18] As the reaction temperature decreases, the intensity of the Cr deposits decreased significantly. For the O_2 reduction reaction at 700 °C, isolated fine particles were formed on the YSZ electrolyte surface area between the original LSM particles with no preferential deposition at the LSM electrode/YSZ electrolyte interface [Fig. 8(c)], similar to the initial deposition of Cr species at 900 °C (Fig. 2). The large and

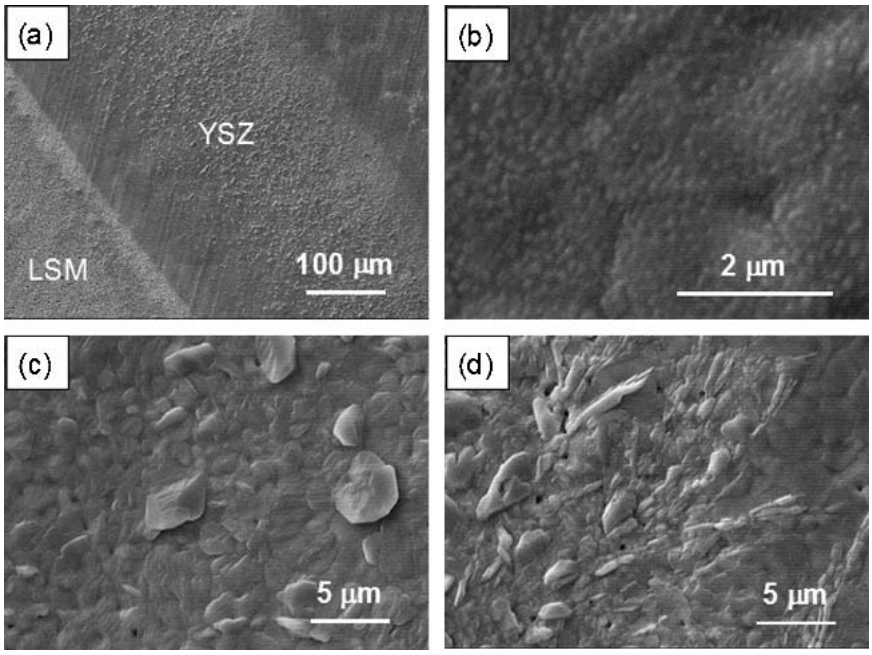

FIG. 5. SEM micrographs of the Cr deposits on the YSZ electrolyte surface not in contact with the LSM electrode after cathodic current passage at 900 °C for 20 h under the rib of the interconnect: (a) Overview of the YSZ electrolyte surface, showing the formation of a band close to the edge of the LSM electrode, (b) ~20 μm next to the edge of LSM, (c) ~50 μm away from the edge of LSM, and (d) ~250 μm away from the edge of LSM.

irregular particles were LSM left on the YSZ electrolyte surface. On the isolated fine particles, EDS analysis clearly showed the presence of Cr and probably Mn [Fig. 9(c)].

Figure 10 shows the initial impedance response of the LSM electrodes as a function of a cathodic current passage of 200 mA cm^{-2} at different temperatures in air in the presence of a Fe–Cr alloy. In general, the electrode impedance decreases with the cathodic current passage. However, the relative degree in the reduction of the electrode impedance varies with the temperature. At 900 °C in the presence of chromia-forming alloy [Fig. 10(a)], the size of the impedance arcs fluctuated with cathodic current passage. For the reaction at 800 °C, electrode polarization resistance R_E was reduced from an initial value of 13.2 to 3.6 Ωcm^2 after the cathodic current passage for 240 min [Fig. 10(b)], a 72% reduction in R_E. At 700 °C, the initial value of R_E was 77.1 Ωcm^2, and it was reduced to 47.3 Ωcm^2 after 120 min cathodic current passage. R_E was reduced by 39%. The reduction in the electrode polarization resistance for the O_2 reduction in the presence of Fe–Cr alloy was also reported by Matsuzaki and Yasuda.[14] As shown previously, the reduction in the electrode polarization resistance measured at open circuit in the presence and absence of Fe–Cr alloy is most likely due to the significant activation effect of the cathodic polarization on the initial electrode behavior of the freshly-prepared LSM electrodes.[15,23,24]

Different from the electrode impedance behavior at open circuit, the polarization potential for the O_2 reduction reaction on the LSM electrodes in the presence of Fe–Cr alloy increases with the cathodic current passage time, as shown in Fig. 11. In the presence of chromia-forming alloy, the polarization behavior was characterized by two distinct regions, a rapid rise region I and a potential plateau region II, as shown in Fig. 11(a). The change of the polarization potential $E_{cathode}$ with the cathodic current passage time was quite reproducible at the temperature ranges studied. Such behavior at the early stage of the reaction in the presence of Fe–Cr alloy has been explained by the strong inhibiting effect of the gaseous Cr species on the surface process such as the dissociate adsorption and diffusion reaction on the electrode surface for the O_2 reduction reactions.[15,16] The increase of polarization potential was mainly due to the increase of overpotential (η), as indicated by the stable electrode ohmic resistance R_Ω of the electrode. For the reaction in the presence of Fe–Cr alloy, η at 200 $mAcm^{-2}$ was 613 mV after cathodic polarization for 240 min at 900 °C. Under the same polarization conditions, η was 685 and 785 mV at 800 and 700 °C, respectively. Thus, the lower the temperature, the higher the overpotential for the O_2 reduction reaction on the LSM electrode in the presence of Fe–Cr alloy. This is consistent with the high activation energy for the O_2 reduction reaction on the LSM-based electrode materials.[25]

IV. DISCUSSION

As shown in Fig. 2, Cr deposition on the LSM electrode and YSZ electrolyte interface regions increases

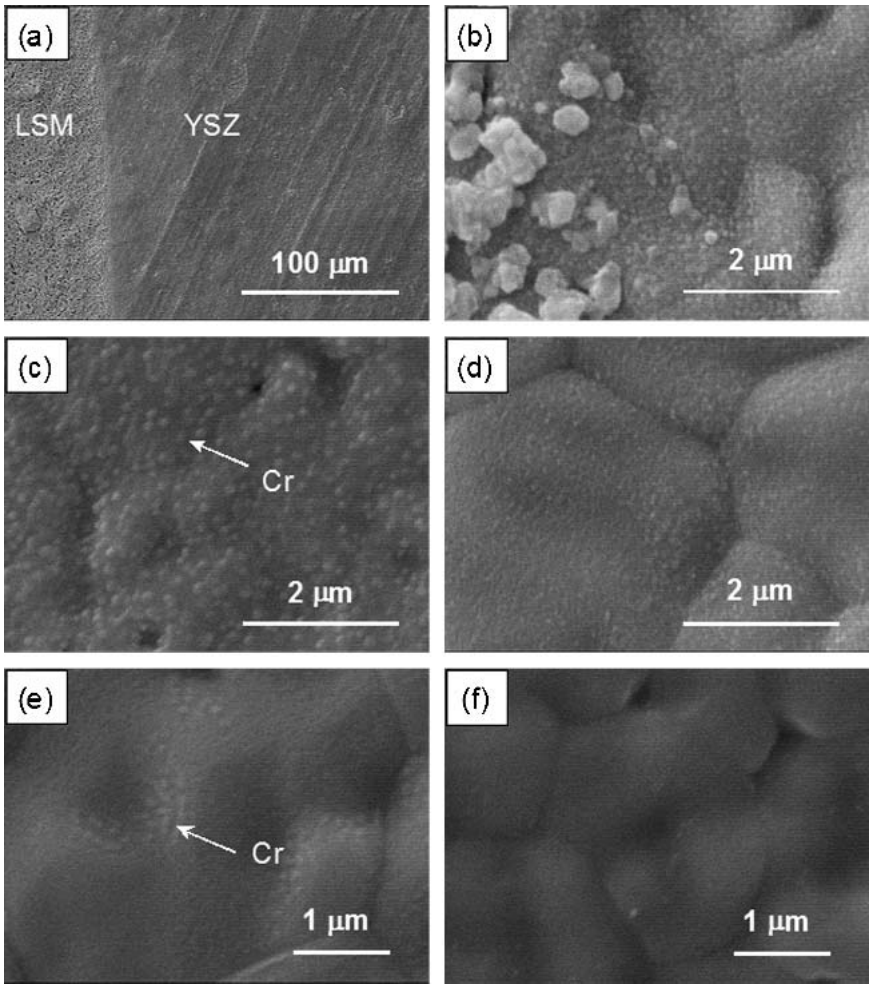

FIG. 6. SEM micrographs of the Cr deposits on the YSZ electrolyte surface not in contact with the LSM electrode after cathodic current passage at 900 °C for 20 h under the channel of the interconnect: (a) overview of the YSZ electrolyte surface, showing no clear formation of the deposit band at the edge of the LSM electrode; (b) next to the edge of LSM; (c) ~20 μm next to the edge of LSM; (d) ~50 μm away from the edge of LSM; (e) ~70 μm away from the edge of LSM; and (f) YSZ electrolyte surface without deposit.

with the cathodic polarization time at 900 °C. This is widely known and well documented in the literature.[12,17] However, the distribution of the Cr deposits on the YSZ system observed at the early stage of the reaction shows no preferential deposition of Cr species at the areas around the convex rings [Figs. 2(a) and 2(b)]. Atomic force microscopy (AFM) studies of the formation of the convex rings at the O_2/LSM/YSZ interface and the subsequent broadening under both cathodic and anodic polarization conditions indicate that convex rings are most likely the three phase boundary regions for the O_2 reduction reactions.[26] Random Cr deposition on the YSZ electrolyte surface between the LSM particles was also observed for the reaction at 700 °C [Fig. 8(c)]. Cr particles simply filled the YSZ electrolyte surface space between LSM grains as the polarization time increased. On the other hand, the relative increase in the cathodic potential ($E_{cathode}$) with the cathodic current passage is quite reproducible despite the continued accumulation of the Cr deposits at the LSM electrode and YSZ electrolyte interface. For example, for the reaction at 900 °C, the relative increase in $E_{cathode}$ after the cathodic current passage for 240 min was 397 mV, close to 345 mV after the cathodic polarization for 5 min. The relative increase in $E_{cathode}$ was measured by the difference between the initial $E_{cathode}$ when current was applied and the $E_{cathode}$ value at the potential plateau. In comparison, the Cr deposition on the LSM/YSZ interface after the cathodic current passage for 240 min was far more significant than that after the cathodic polarization for only 5 min [Figs. 2(a) and 2(d)]. This shows that there is no intrinsic relationship between the Cr deposition and the oxygen activity or the O_2 reduction reaction at the three phase boundaries in contrast to the proposed electrochemical deposition mechanism of Cr species.[12–14] Rather, Cr deposition is basically controlled by the chemical dissociation, initiated by the nucleation reaction between the gaseous Cr species and manganese species in particular Mn^{2+}.[18–20]

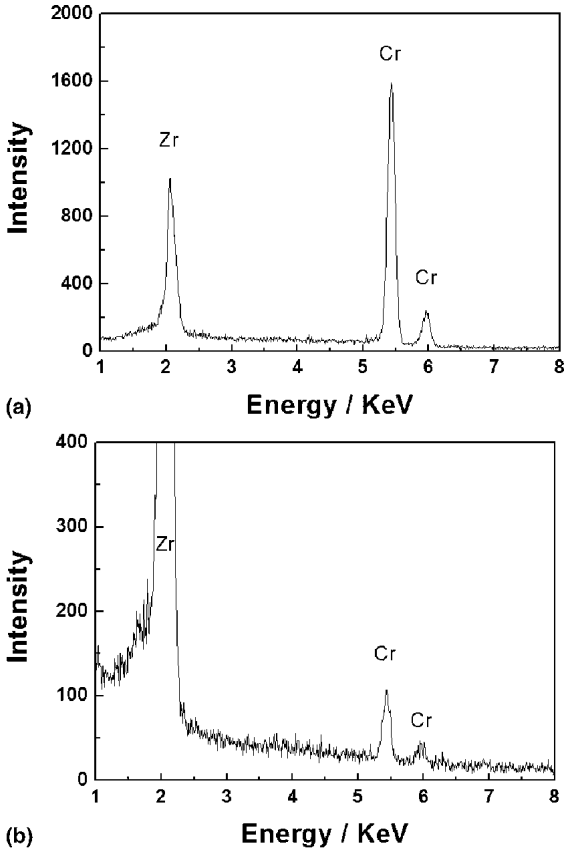

FIG. 7. EDS patterns of the Cr deposits on the YSZ electrolyte surface under (a) the rib [Fig. 5(c)] and (b) the channel [Fig. 6(c)] of the interconnect.

Mn in the LSM lattice and interstitial sites can be electrochemically reduced to Mn^{2+} ions, forming concomitantly oxygen vacancies[27,28]

$$2Mn^{3+} + O_o^x\ (LSM) + 2e \rightarrow 2Mn^{2+} + V_o^{\bullet\bullet} + O_o^x(electrolyte) \quad , \qquad (2)$$

where O_o^x is a normal oxygen interstitial or lattice site and V_o^x is the corresponding oxygen vacancy. Manganese ions such as Mn^{2+} are known to be mobile under high temperature and cathodic polarization conditions.[29,30] Thus, the interaction between the mobile Mn^{2+} ions and gaseous CrO_3 species would lead to the formation of Cr–Mn–O nuclei. However, the nucleation reaction and subsequent grain growth of Cr deposits are kinetically controlled by the contact frequencies and contact time between Mn^{2+} ions and CrO_3 species, which would be highest on the YSZ electrolyte surface close to the edge of the LSM electrode and inside the steps on the electrolyte.[18] The best example is probably the observation of the Cr deposits on the concave surface rather than on the convex surface on the YSZ grains [Fig. 6(e)]. The formation of stable Cr–Mn–O nuclei phases in turn accelerates the crystallization and grain growth of Cr_2O_3 and $(Cr,Mn)_3O_4$ solid phases. The

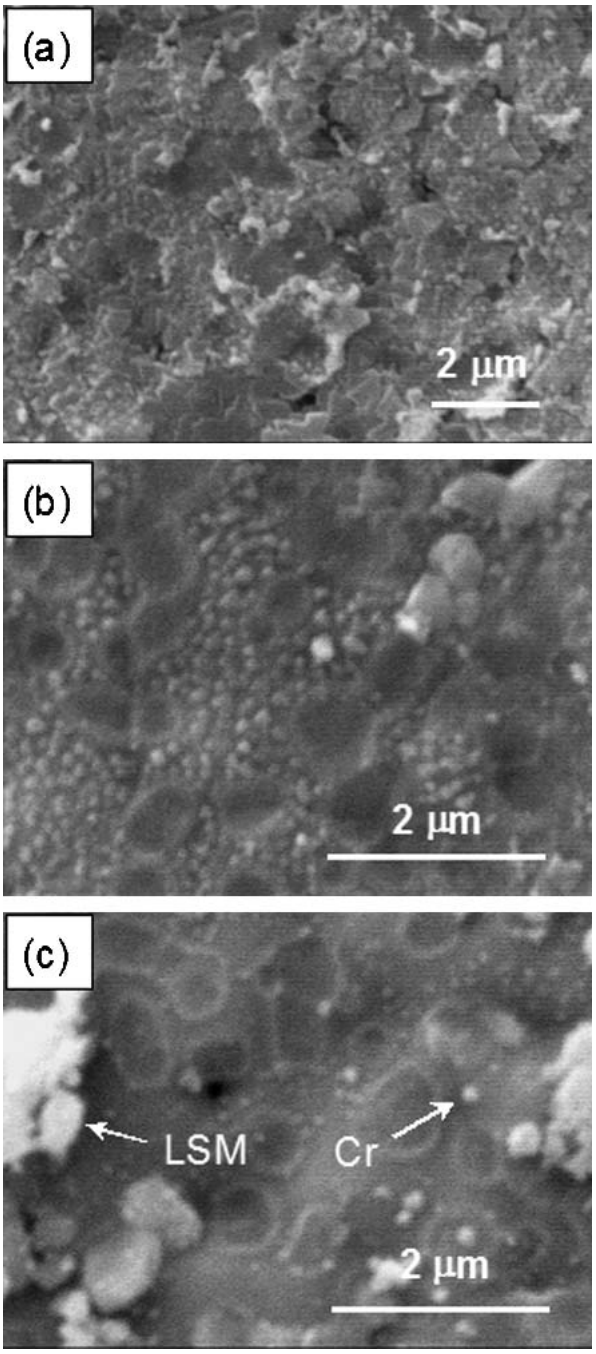

FIG. 8. SEM micrographs of the YSZ electrolyte surface in contact with LSM electrode under the rib of the Fe-Cr interconnect after cathodic currant passage at 200 $mAcm^{-2}$ for 20 h at (a) 900 °C, (b) 800 °C, and (c) 700 °C. LSM electrode coating after polarization at 800 and 700 °C was removed by a doctor blade.

nucleation and grain growth steps can be simply written as follows[18]

$$Mn^{2+} + CrO_3 \rightarrow Cr\text{-}Mn\text{-}O\ (nuclei) \qquad (3)$$

$$Cr\text{-}Mn\text{-}O\ (nuclei) + CrO_3 \rightarrow Cr_2O_3 \qquad (4)$$

$$Cr\text{-}Mn\text{-}O\ (nuclei) + CrO_3 + Mn^{2+} \rightarrow (Cr,Mn)_3O_4 \quad . \qquad (5)$$

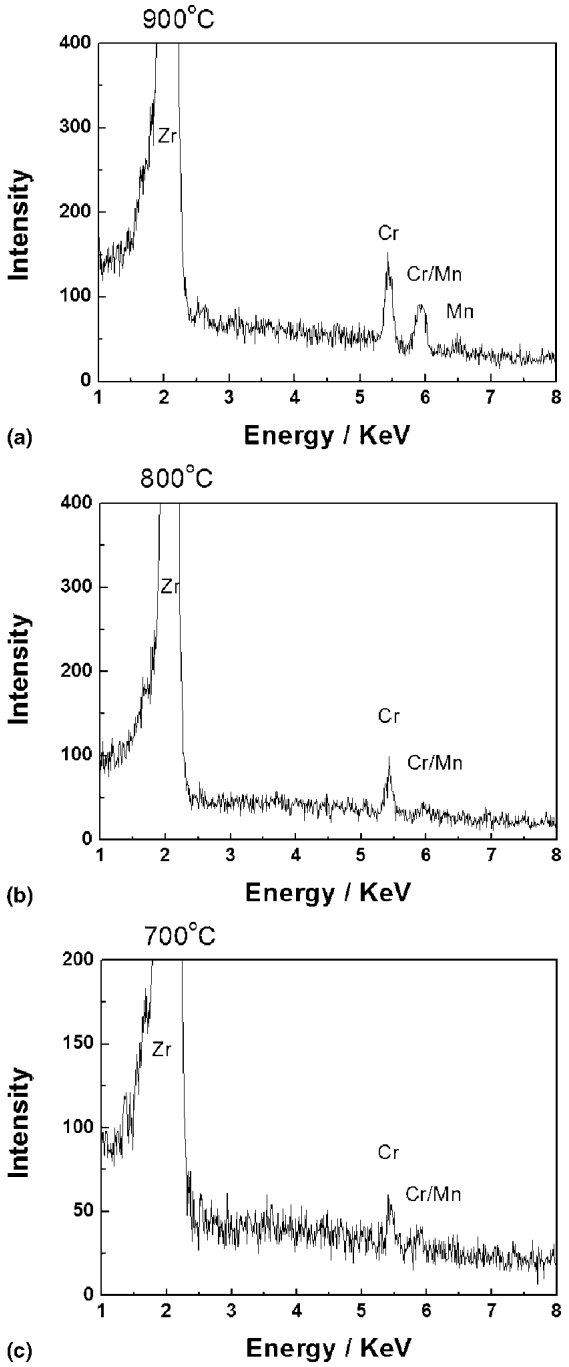

FIG. 9. EDS patterns of Cr deposits on the YSZ electrolyte surface of Fig. 8: (a) at 900 °C, (b) 800 °C, and (c) 700 °C.

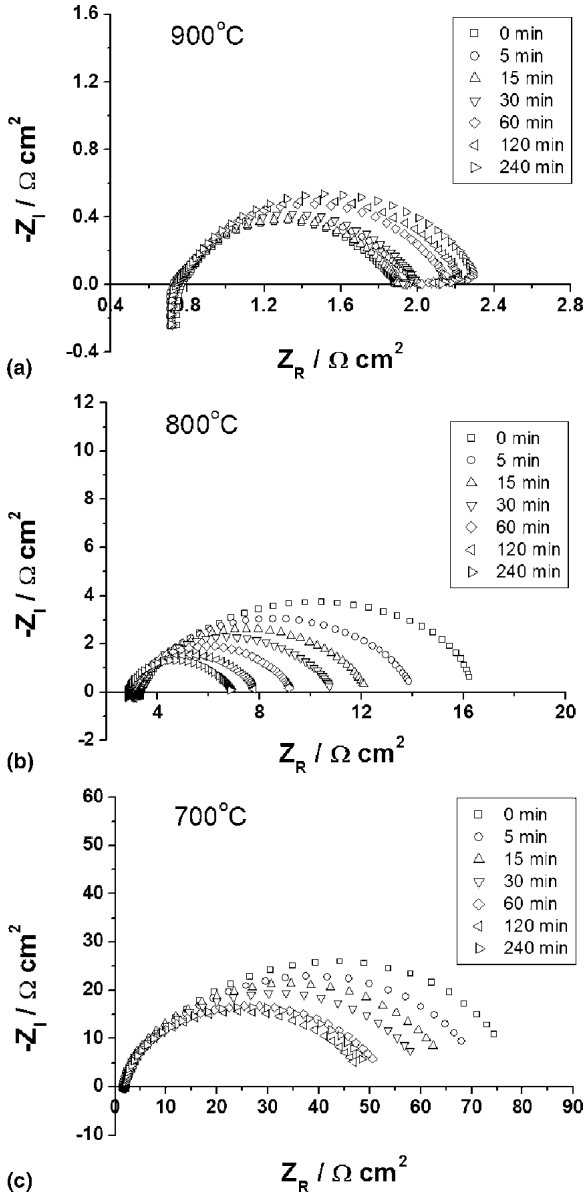

FIG. 10. Initial impedance response of the LSM electrodes as a function of a cathodic current passage time of 200 mA cm^{-2} in the presence of the Fe-Cr alloy interconnect at (a) 900 °C, (b) 800 °C, and (c) 700 °C.

Thus the formation of $(Cr,Mn)_3O_4$-type spinel would be facile if there is sufficient supply of Mn^{2+} ions. Figure 12 shows schematically the deposition processes of Cr species at the LSM/YSZ system under the cathodic polarization conditions in the presence of Fe–Cr alloy metallic interconnect. As the mechanism of the Cr deposition under the SOFC operation conditions is chemical in nature, the nucleation and grain growth of the Cr deposits can occur on the YSZ electrolyte surface with and without the direct contact with the LSM electrode (Figs. 2, 5, and 6). It is just coincident that for the O_2 reduction on the LSM cathode, the generation of Mn^{2+} is directly related to the cathodic polarization via the generation of the oxygen vacancies. This in turn leads to the increased Cr deposition with the cathodic polarization potential. This explains the observed phenomena of the relationship between the Cr deposition at the LSM/YSZ interface region and the cathodic polarization.

The intensity and amount of Cr deposition are significantly related to the flow field design of the interconnect. The significant difference in the Cr deposition on the

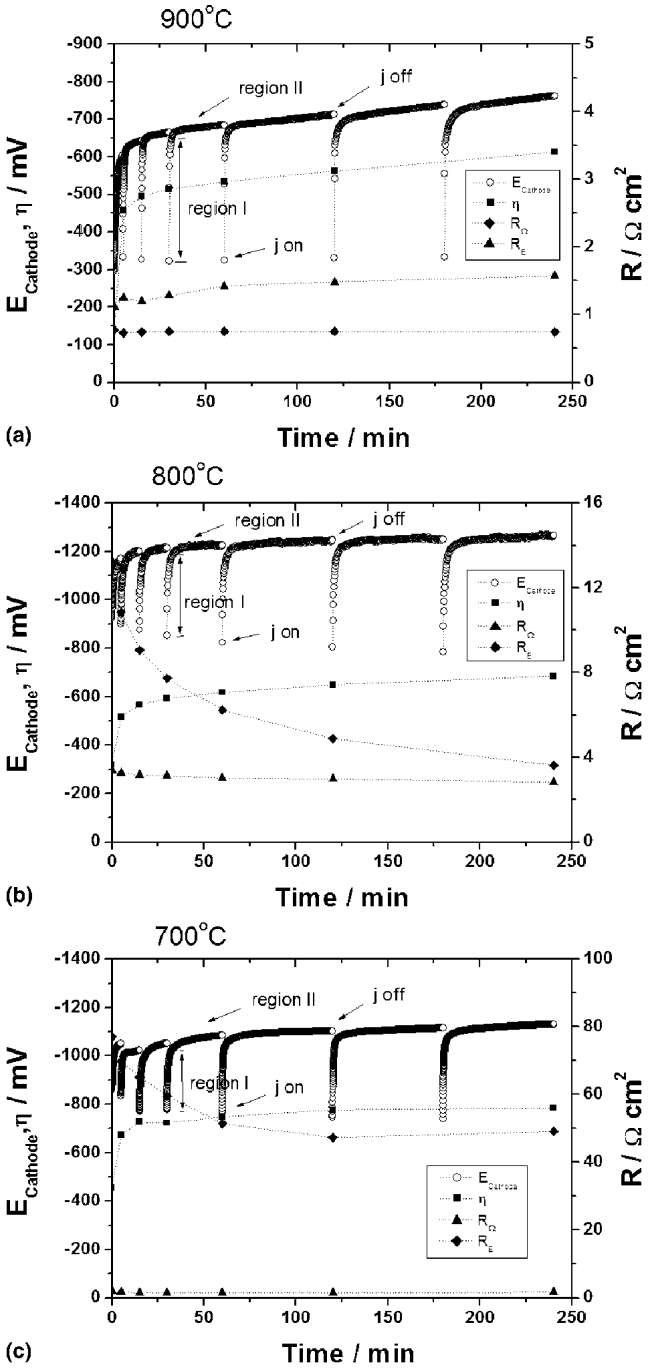

FIG. 11. Initial polarization curves of the LSM electrodes as a function of a cathodic current density of 200 mA cm^{-2} in the presence of Fe-Cr alloy interconnect at (a) 900 °C, (b) 800 °C, and (c) 700 °C. The electrode polarization resistance (R_E) was taken from the impedance measured at open circuit (Fig. 10).

YSZ surface under the rib and channel of the metallic interconnect can be explained by the difference in the flux of Cr species.[19] The distance between the YSZ and the interconnect surface under the rib was equal to thickness of the LSM coating (~20 μm), while the distance between the YSZ and the interconnect surface under the channel was equal to the channel depth plus the coating thickness (~1220 μm). It has been shown that for the oxidation and vaporization of Cr_2O_3, a stagnant gaseous boundary layer is formed adjacent to the chromia surface and the mass transport through the gaseous boundary layer is a rate-limiting step for the oxidation and vaporization of Cr_2O_3.[11,31] Thus, for the area under the channel of the interconnect, air flow would greatly reduce the thickness of the gaseous boundary layer and sweep away Cr species. This in turn reduces significantly the flux of Cr species at the YSZ/LSM interface areas under the channel of the interconnect. On the other hand, the Cr flux at the YSZ/LSM interface area under the rib of the interconnect would be much less affected by the air flow and the distance for the flux of the Cr species is also much shorter. As the migration of manganese species (e.g., Mn^{2+}) generated under the cathodic polarization is mainly through surface diffusion and should not be affected significantly by the air flow, the deposition of the Cr would be far more significant on the YSZ surface under the rib of the interconnect due to the much higher Cr flux, as compared to that under the channels of the interconnect.

The deposition of Cr under the cathodic polarization conditions depends strongly on the reaction temperature (Fig. 8). The deposition of Cr species at 700 °C is drastically lower than that at 900 °C under the same cathodic current passage conditions. As shown by Hilpert et al.,[10] CrO_3 is one of the main gaseous Cr species over chromium oxide scale under dry and humidified air and partial pressure of CrO_3 decreases with the decrease in temperature. The partial pressure of CrO_3 is about 1.39×10^{-3} Pa at 900 °C while at 700 °C it decreases to 9.73×10^{-6} Pa. On the other hand, the supply of the Mn^{2+} generated under cathodic polarization potentials could also be significantly reduced at low temperatures. Cation diffusion in the perovskite oxides is known to be very slow. The diffusion coefficient of cations such as La and Mn in $(LaSr)(GaMg)O_3$ perovskite was in the range of 10^{-13} cm^2 s^{-1} at 1400 °C.[32] At 900 °C the cation diffusion in the $(LaCa)CrO_3$ perovskite bulk phase can be calculated to be 10^{-16} cm^2 s^{-1} and at 700 °C, it would decrease to 10^{-19} cm^2 s^{-1} due to the high activation energy of the cation diffusion in the perovskite.[33] Thus, reduction in the reaction temperature not only reduces the partial pressure of Cr species but also the diffusivities of manganese species (e.g., Mn^{2+}) in the LSM-based perovskite. This in turn would lead to the reduced nucleation reaction and subsequent grain growth reactions between the manganese and Cr species. This appears to be supported by the substantial reduction in the deposition of Cr species on the YSZ electrolyte surface at reduced reaction temperatures despite the increase in the overpotentials for the reaction (Figs. 8 and 11).

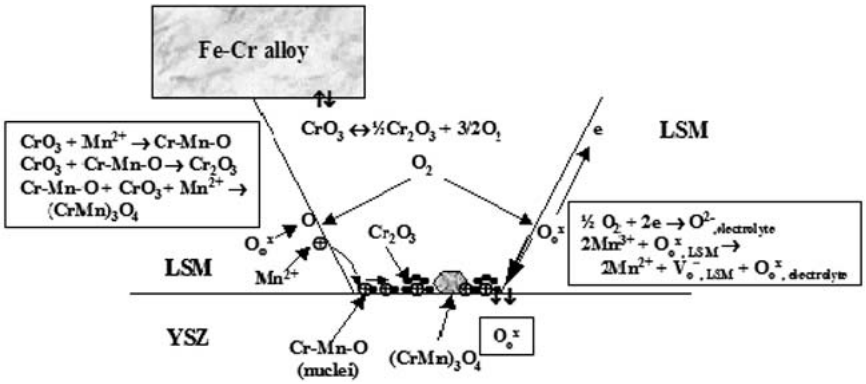

FIG. 12. Scheme of the Cr deposition reaction at LSM cathode and YSZ electrolyte in the presence of Fe–Cr alloy metallic interconnect under SOFC operation conditions.

V. CONCLUSION

The deposition process of Cr species at the LSM electrode/YSZ electrolyte/Fe–Cr alloy metallic interconnect system has been investigated under a constant cathodic current passage of 200 mA cm^{-2} in the early stages of the reaction. Cr species show no preferential deposition at the three phase boundary of O_2, LSM electrode and YSZ electrolyte. Rather, deposition of Cr species on the YSZ electrolyte surface is random at the early stage of the reaction in the presence of Fe–Cr alloy interconnect. The results demonstrate again that the deposition of Cr species at the LSM electrode is not an electrochemical reduction reaction of high valent Cr species to solid Cr_2O_3 at the three-phase boundary region in competition with O_2 reduction.

The substantial reduction in the Cr deposition at the LSM electrode and YSZ electrolyte at reduced temperature is most likely due to the significant decrease in the cation diffusivities in LSM-based perovskite oxides and the partial pressure of gaseous Cr species.

ACKNOWLEDGMENT

Y.D. Zhen thanks the Nanyang Technological University for the graduate research studentship.

REFERENCES

1. N.Q. Minh and T. Takahashi: *Science and Technology of Ceramic Fuel Cells* (Elsevier, Amsterdam, The Netherlands, 1995).
2. L.C. De Jonghe, C.P. Jacobson, and S.J. Visco: Supported electrolyte thin film synthesis of solid oxide fuel cells. *Ann. Rev. Mater. Res.* **33,** 169 (2003).
3. S.P. Jiang, S. Zhang, Y.D. Zhen, and A.P. Koh: Performance of GDC-impregnated Ni anodes of solid oxide fuel cells. *Electrochem. Solid-State Lett.* **7,** A282 (2004).
4. E.P. Murray, T. Tsai, and S.A. Barnett: A direct-methane fuel cell with a ceria-based anode. *Nature* **400,** 649 (1999).
5. Z. Shao and S.M. Haile: A high performance cathode for the next generation of solid-oxide fuel cells. *Nature* **431,** 170 (2004).
6. W.Z. Zhu and S.C. Deevi: Opportunity of metallic interconnects for solid oxide fuel cells: A status on contact resistance. *Mater. Res. Bull.* **38,** 957 (2003).
7. K. Huang, P.Y. Hou, and J.B. Goodenough: Characterization of iron-based alloy interconnects for reduced temperature solid oxide fuel cells. *Solid State Ionics* **129,** 237 (2000).
8. T. Horita, Y. Xiong, K. Yamaji, N. Sakai, and H. Yokokawa: Evaluation of Fe-Cr alloys as interconnects for reduced operation temperature SOFCs. *J. Electrochem. Soc.* **150,** A243 (2003).
9. T. Brylewski, M. Nanko, T. Maruyama, and K. Przybylski: Application of Fe-16Cr ferric alloy to interconnector for a solid oxide fuel cell. *Solid State Ionics* **143,** 131 (2001).
10. K. Hilpert, D. Das, M. Miller, D.H. Peck, and R. Weiß: Chromium vapor species over solid oxide fuel cell interconnect materials and their potential for degradation processes. *J. Electrochem. Soc.* **143,** 3642 (1996).
11. H.G. Graham and H.H. Davis: Oxidation/vaporization kinetics of Cr_2O_3. *J. Am. Ceram. Soc.* **54,** 89 (1971).
12. S. Taniguchi, M. Kadowaki, H. Kawamura, T. Yasuo, Y. Akiyama, Y. Miyake, and T. Saitoh: Degradation phenomena in the cathode of a solid oxide fuel cell with an alloy separator. *J. Power Sources* **55,** 73 (1995).
13. S.P.S. Badwal, R. Deller, K. Foger, Y. Ramprakash, and J.P. Zhang: Interaction between chromia forming alloy interconnects and air electrode of solid oxide fuel cells. *Solid State Ionics* **99,** 297 (1997).
14. Y. Matsuzaki and I. Yasuda: Electrochemical properties of a SOFC cathode in contact with a chromium-containing alloy separator. *Solid State Ionics* **132,** 271 (2000).
15. S.P. Jiang, J.P. Zhang, and K. Foger: Deposition of chromium species at Sr-doped $LaMnO_3$ electrodes in solid oxide fuel cells. II. Effect on O_2 reduction reactions. *J. Electrochem. Soc.* **147,** 3195 (2000).
16. S.P. Jiang: Use of gaseous Cr species to diagnose surface and bulk process for O_2 reduction in solid oxide fuel cells. *J. Appl. Electrochem.* **31,** 181 (2001).
17. Y. Matsuzaki and I. Yasuda: Dependence of SOFC cathode degradation by chromium-containing alloy on compositions of electrodes and electrolytes. *J. Electrochem. Soc.* **148,** A126 (2001).
18. S.P. Jiang, J.P. Zhang, L. Apateanu, and K. Foger: Deposition of chromium species at Sr-doped $LaMnO_3$ electrodes in solid oxide fuel cells. I. Mechanism and kinetics. *J. Electrochem. Soc.* **147,** 4013 (2000).
19. S.P. Jiang, J.P. Zhang, and K. Foger: Deposition of chromium species at Sr-doped $LaMnO_3$ electrodes in solid oxide fuel cells. III. Effect of air flow. *J. Electrochem. Soc.* **148,** C447 (2001).

20. S.P. Jiang, J.P. Zhang, and X.G. Zheng: A comparative investigation of chromium deposition at air electrodes of solid oxide fuel cells. *J. Eur. Ceram. Soc.* **22,** 361 (2002).
21. S.P. Jiang, J.P. Zhang, Y. Ramprakash, D. Milosevic, and K. Wilshier: An investigation of shelf-life of strontium doped $LaMnO_3$ materials. *J. Mater. Sci.* **35,** 2735 (2000).
22. A. Mitterdorfer and L.J. Gauckler: $La_2Zr_2O_7$ formation and oxygen reduction kinetics of the $La_{0.85}Sr_{0.15}Mn_yO_3$, O_2 (g)|YSZ system. *Solid State Ionics* **111,** 185 (1998).
23. S.P. Jiang, J.G. Love, J.P. Zhang, M. Hoang, Y. Ramprakash, A.E. Hughes, and S.P.S. Badwal: The electrochemical performance of LSM/zirconia-yttria interface as a function of A-site non-stoichiometry and cathodic current treatment. *Solid State Ionics* **121,** 1 (1999).
24. S.P. Jiang and J.G. Love: Origin of the initial polarization behavior of Sr-doped $LaMnO_3$ for O_2 reduction in solid oxide fuel cells. *Solid State Ionics* **138,** 183 (2001).
25. S.P. Jiang, J.G. Love, and Y. Ramprakash: Electrode behaviour at the (La,Sr)MnO_3/Y_2O_3-ZrO_2 interface by electrochemical impedance spectroscopy. *J. Power Sources* **110,** 201 (2002).
26. S.P. Jiang and W. Wang: Effect of polarization on the interface between (La,Sr)MnO_3 electrode and Y_2O_3-ZrO_2 electrolyte. *Electrochem. Solid-State Lett.* **8,** A115 (2005).
27. H.Y. Lee, W.S. Cho, S.M. Oh, H-D. Wiemhöfer, and W. Göpel: Active reaction sites for oxygen reduction in $La_{0.9}Sr_{0.1}MnO_3$/YSZ electrodes. *J. Electrochem. Soc.* **142,** 2659 (1995).
28. X.J. Chen, S.H. Chan, and K.A. Khor: Defect chemistry of $La_{1-x}Sr_xMnO_3$ under cathodic polarization. *Electrochem. Solid-State Lett.* **7,** A144 (2004).
29. A. Weber, R. Männer, B. Jobst, M. Schiele, H. Cerva, R. Waser, and E. Ivers-Tiffée: In *Proc. 17th Riso Int. Symp. Mater. Sci. High Temperature Electrochemistry: Ceramics and Metals*, edited by F.W. Poulsen, N. Bonanos, S. Linderoth, M. Mogensen and B. Zacharau-Christiansen (Risø National Laboratory, Roskilde, Denmark, 1996), p. 473.
30. S.P. Jiang, J-P. Zhang, and K. Föger: Chemical interaction between 3 mol% yttria-zirconia and Sr-doped lanthanum mangnite. *J. Eur. Ceram. Soc.* **23,** 1865 (2003).
31. C.A. Stearns, F.K. Kohl, and G.C. Fryburg: Oxidative vaporization kinetics of Cr_2O_3 in oxygen from 1000 to 1300 °C. *J. Electrochem. Soc.* **121,** 945 (1974).
32. O. Schulz and M. Martin: Preparation and characterization of $La_{1-x}Sr_xGa_{1-y}Mg_yO_{3-(x+y)/2}$ for the investigation of cation diffusion processes. *Solid State Ionics* **135,** 549 (2000).
33. T. Horita, M. Ishikawa, K. Yamaji, N. Sakai, H. Yokokawa, and M. Dokiya: Cation diffusion in (La,Ca)CrO_3 perovskite by SIMS. *Solid State Ionics* **108,** 383 (1998).